NASA TECHNICAL NOTE

NASA TN D-3470



NASA TN D-3470

# ATMOSPHERIC TRACKING ERRORS AT S- AND C-BAND FREQUENCIES

*by P. E. Schmid*

*Goddard Space Flight Center*
*Greenbelt, Md.*



NATIONAL AERONAUTICS AND SPACE ADMINISTRATION • WASHINGTON, D. C. • AUGUST 1966

# ATMOSPHERIC TRACKING ERRORS AT S- AND C-BAND FREQUENCIES

By P. E. Schmid

Goddard Space Flight Center
Greenbelt, Md.

NATIONAL AERONAUTICS AND SPACE ADMINISTRATION

For sale by the Clearinghouse for Federal Scientific and Technical Information
Springfield, Virginia 22151 – Price $2.00

## ABSTRACT

The primary purpose of this paper is to provide a realistic estimate of the errors introduced in microwave ranging measurements as a result of diurnal, seasonal, and annual changes in the earth's atmosphere. This analysis, which is based upon the extensive atmospheric investigations described in the literature, is directly applicable to such systems as the Unified S-band System which will be employed in the forthcoming Apollo Missions. The effects of both the troposphere and ionosphere upon measurements of range, range-rate and elevation angle are discussed.

CONTENTS


Abstract . . . . . ii

INTRODUCTION . . . . . 1

TROPOSPHERIC ERRORS . . . . . 5

General . . . . . 5

Tropospheric Elevation Angle Error . . . . . 8

Tropospheric Range Error . . . . . 11

Tropospheric Range-Rate Error . . . . . 13

IONOSPHERIC ERRORS . . . . . 18

General . . . . . 18

Ionospheric Elevation Angle Error . . . . . 20

Ionospheric Range Error . . . . . 22

Ionospheric Range-Rate Error . . . . . 24

CONCLUSIONS . . . . . 26

Atmospheric Induced Error for Vehicle Heights Above 200 km . . . . . 26

Influence of the Atmosphere at the Nominal Apollo Unified S-Band Frequency of 2 kMc . . . . . 27

ACKNOWLEDGMENT . . . . . 29

References . . . . . 29

Appendix A—Glossary . . . . . 33

# ATMOSPHERIC TRACKING ERRORS AT S- AND C-BAND FREQUENCIES

by
P. E. Schmid
*Goddard Space Flight Center*

## INTRODUCTION

During the past decade considerable effort by many independent investigators has been directed toward the theoretical study and analysis of the effect of the atmosphere upon microwave radio propagation. A number of mathematical models of the atmosphere have been devised in an attempt to estimate the influence of the earth's atmosphere upon measurements of range, range rate, and elevation angle of earth satellite and space vehicle tracking systems. To a certain extent the sysmatic or biasing effects of the atmosphere are predictable and can be corrected for if sufficient data regarding the atmospheric state are available. This paper examines the error, attributed to an imperfect knowledge of the atmosphere, that occurs while using microwave energy to observe spacecraft at altitudes greater than 200 km above the earth. To the extent possible experimental verifications of the atmospheric models cited are presented.

The effects of the troposphere and ionosphere upon radiowave propagation can best be predicted if an accurate refractivity profile of the atmosphere is available. Thus one approach to obtaining correction data is based upon atmospheric refraction profile measurements just prior to a tracking operation and a subsequent ray tracing by means of a digital computer (Reference 1).

A second approach is to base tropospheric corrections on surface refractivity measurements (which can again be performed just prior to tracking) and, as discussed in the section entitled "Ionospheric Errors," upon the average state of the ionosphere. In this approach a mathematical model of the atmosphere must be used and the correction is, of course, no better than the model. The accuracy of the National Bureau of Standards Central Radio Propagation Laboratory exponential model troposphere has been verified by means of experiments which permit a comparison of calculated and measured angles of arrival of solar microwave radio energy.

Figure 1 shows the mean total measured refraction of solar radio energy at 16.2 kMc and 34.5 kMc compared with that calculated with the exponential model. The 16.2 kMc measurements (References 2 and 3) were conducted to examine the accuracy of the National Bureau of Standards exponential model prediction equations through a comparison with some precise measurements of total absolute refraction made with a radio sextant by the Collins Radio Company. This radio sextant consisted of a high-gain, narrow-beamwidth antenna which automatically tracked the radio

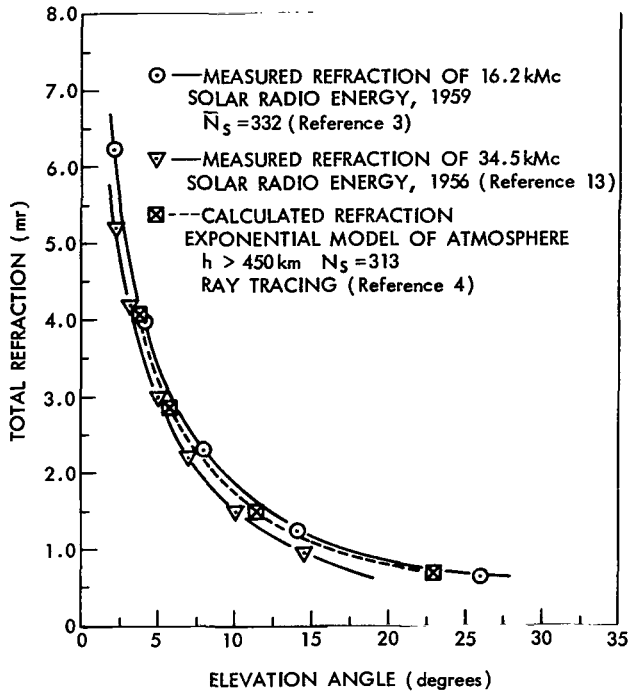


Figure 1—Atmospheric refraction of solar radio energy.

noise emanating from the sun's disc by means of continuous circular scanning. This principle is a common technique in radar automatic angle tracking whereby the antenna feedpoint is mutated (either mechanically or electronically) to cause a slight excursion of the spacial antenna pointing while the main antenna structure or dish, in the absence of any received signal at the antenna aperture, remains fixed. In the 2 cm wavelength microwave region, the sun radiates thermal noise energy similar to a blackbody having a temperature of approximately 7000°K. With the output of the high-gain antenna connected to a sensitive microwave receiver, the maximum signal output occurred when the scanning antenna pattern was centered upon the sun's disc. As the antenna scanned off axis, the receiver output dropped to zero and an error voltage was generated which caused the antenna drive motors to redirect the antenna beam toward the sun's center.

The assumption that radio energy is uniformly generated over the sun's surface is valid except during times of anomalous sunspot activity. Fortunately such sunspot activity is easily discerned by the nature of the receiver output and consequently any data recorded during such periods was disregarded. The radio sextant-measured pointing was compared to calculated positions of the sun based on highly accurate ephemeris data supplied by the U.S. Naval Observatory. A thorough discussion of the error analysis associated with the approximately 40000 separate refraction measmade over a five month period with the radio sextant is presented in Reference 2. A thorough discussion of the exponential mathematical model for the troposphere as well as related topics is given in Reference 4.

A third approach to atmospheric correction is to use average atmospheric data without regard for diurnal or seasonal meteorological fluctuations. The latter technique, as will be shown, can result in appreciable measurement error at low elevation angles.

The angle of arrival measurement of radio energy from the sun is an example of a test designed to investigate the absolute accuracy of the exponential mathematical model of the troposphere. The refraction in this case is attributed solely to the troposphere since the solar radio energy at 16.2 kMc is well above those frequencies affected by the ionosphere. The exponential model can also be checked by comparing calculated and measured refractivity profiles. Figure 2 shows a typical measured profile obtained at Valkaria, Florida, by means of a radiosonde (Reference 5) compared to the exponential model based on a measure of the refractivity at the surface and at a height of 1 km above the surface. The two curves are seen to coincide from 0 to 5 km and show a

maximum deviation, $\Delta N$, of about 10 at 12 km. Field tests have indicated that refraction corrections based upon refractometer profiles, radiosonde profiles and exponential model profiles are calculable to about 1.6 percent on a statistical basis (Reference 6). In terms of elevation angle error remaining after attempted correction, this amounts to ±0.04 mr at 5° elevation. In the section entitled "Tropospheric Errors" it is shown that this error decreases rapidly with increasing elevation. The statistical fluctuations in the correction procedure are largely due to the time-dependent variations of the refractive index profile. The variations in surface refractivity are directly related to overall tropospheric profile variations, and hence to the error introduced in ranging measurements, by means of the exponential profile ray tracings of B. R. Bean and G. D. Thayer (Reference 4).

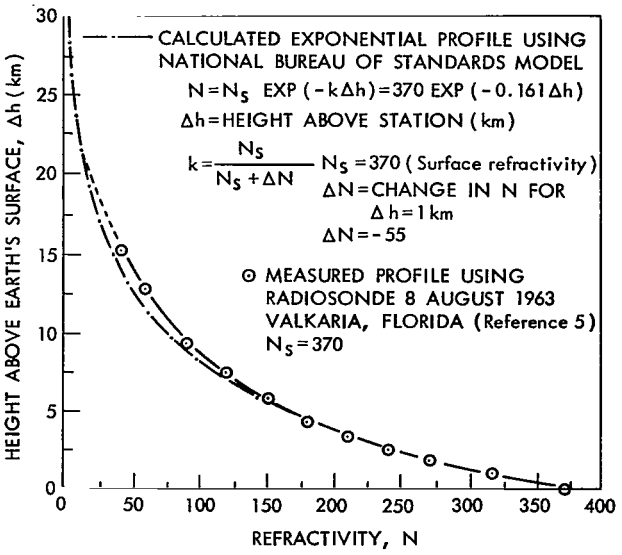


Figure 2—Typical measured tropospheric index of refraction profile compared to exponential model.

In most of the tropospheric models described in the literature, the effects upon radio wave propagation are related to surface refractivity, $N_s$. Thus, if the model is appropriate at a particular value of $N_s$ and a compensating correction is made to ranging data, it is of interest to note the deviations from this correction, which might be anticipated as $N_s$, slowly fluctuates throughout the year. The variations come about as the changing seasons alter the air temperature, total air pressure and air water vapor content. The same parameters are also affected over a much shorter cycle as the air mass is subjected to daily temperature and moisture variations, especially those associated with the transition from local day to night. Thus as shown in Figure 3, the overall pattern of refractivity change during a span of a year is one of slow seasonal variation modified by more rapid diurnal cycles. In the United States the months of May through August are generally those of greatest refractivity fluctuation and the predominant change in $N_s$ during any given month at a particular site can be attributed to diurnal effects.

The National Bureau of Standards has compiled a book of surface refractivity charts and data based upon 8 years of surface weather data from 60 weather stations in the United States and 5 years of surface weather data from 306 worldwide stations (Reference 7). The surface refractivity values tabulated in this publication are derived from measured air temperature, total air pressure and water vapor content. The basic tabulated data for each site within the United States is the 8 year refractivity average

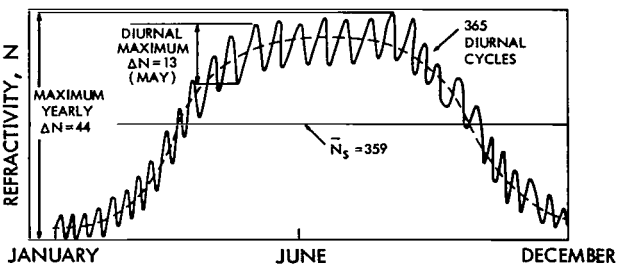


Figure 3—Typical variation in surface refractivity (data from Reference 7, for Miami, Florida).

for a particular time of day during a given month. For example, the 8 year mean value $\bar{N}_s$ at Miami, Florida, for 12 noon during the month of August was 369.4 with a standard deviation of 8.9. This distribution is based on 248 separate refractivity calculations. The mean value as calculated for the even hours of the day clearly traces out the average diurnal cycle associated with each day of a particular month. This average diurnal variation is indicated in Table 1 for seven weather stations which include areas near the tracking stations at Cape Kennedy, Florida; White Sands, New Mexico; Corpus Christi, Texas; Blossom Point, Maryland; Goldstone, California; and E. Grand Forks, Minnesota.

The yearly variation in $N_s$ for each site is presented as the difference between the maximum and minimum monthly value of $\bar{N}_s$. For example, for Miami, Florida, the maximum monthly mean is 381.0 (September for 2200 hours) and the minimum is 336.5 (January for 1400 hours); there is a yearly average change of 44.5. These variations provide an estimate of the magnitude of the future long term fluctuations which can be expected at the geographical locations cited. The distribution of the yearly and diurnal variations is nearly symmetrical and therefore the changes about the best yearly average or best daily average of $N_s$ will vary approximately as $\pm \Delta N/2$, where $\Delta N$ is the total expected variation indicated in Table 1.

It is indicated in the section entitled "Tropospheric Errors" how often refractivity data must be obtained to assure attainment of a specified degree of accuracy in elevation angle, range, and range-rate measurement. With reference to Table 1, it is seen that a diurnal change in $N_s$ of 20 is seldom exceeded for the sites listed and hence a variation of ±10 or less about the best daily average can be anticipated. Similarly, a yearly change of 56 in $N_s$ is seldom exceeded and a variation of ±28 or less about the best yearly average can be expected for the seven geographical locations listed in Table 1. The maximum error remaining after a correction is made for tropospheric effects is examined by means of ray-tracing techniques for the following cases:

1. A worldwide "standard" correction of $N_s = 313$. Error in knowledge of $N_s$ taken as ±60.
2. A best yearly average of $\bar{N}_s$ at a particular site. For this case the error in knowledge of $N_s$ is assumed as ±28 from the actual value at any given time.
3. A best daily average of $\bar{N}_s$ at a particular site. For this case the error in knowledge of $N_s$ is assumed as ±10 from the actual value at any given time.

At this writing, numerous studies are being undertaken in an effort to simplify the task of obtaining meaningful bias correction terms for application to tracking data. For example, the Air Force Cambridge Research Laboratory, The National Bureau of Standards, and the Mitre Corporation are currently conducting experimental programs in an attempt to attain improved correlation between atmospheric structure and atmospheric refraction effects. Cambridge Research Laboratory is trying to arrive at a system whereby the refraction profile of the troposphere can be more accurately determined by observing prevailing cloud conditions. This laboratory has put meteorological equipment, including a refractometer, aboard a C-130 aircraft which is flown through clouds at Cape Kennedy at altitudes up to 6 km. At the same time a U-2 aircraft flies above the C-130 and photographs the C-130 as well as the prevailing cloud cover. Later the cloud pattern is matched with refractometer readings. It is hoped that a sufficient number of comparisons will be obtained to establish an overall refractivity profile which includes generally neglected effects of cloud cover.

Table 1

Range of Variation in Surface Refractivity ($N_s$).

| Weather Station | Yearly Variation in $N_s$, $\Delta N$ | Average Diurnal Variation in $N_s$, $\Delta N$ | | | | | | | | | | | | Yearly Average, $\bar{N}_s$ |
|---|---|---|---|---|---|---|---|---|---|---|---|---|---|---|
| | | Jan. | Feb. | March | April | May | June | July | Aug. | Sept. | Oct. | Nov. | Dec. | |
| Miami, Florida | 44 | 10 | 6 | 6 | 11 | 13 | 12 | 12 | 13 | 11 | 10 | 10 | 10 | 359 |
| Flagstaff, Arizona | 41 | 6 | 9 | 8 | 11 | 14 | 17 | 14 | 14 | 16 | 16 | 10 | 6 | 246 |
| Brownsville, Texas | 52 | 10 | 12 | 14 | 17 | 16 | 19 | 23 | 22 | 15 | 14 | 11 | 11 | 360 |
| Tampa, Florida | 55 | 14 | 13 | 14 | 16 | 22 | 17 | 14 | 12 | 16 | 17 | 12 | 8 | 356 |
| Washington, D. C. | 56 | 6 | 8 | 9 | 10 | 11 | 14 | 18 | 16 | 16 | 12 | 9 | 6 | 334 |
| Fresno, California | 39 | 6 | 11 | 14 | 20 | 24 | 25 | 26 | 27 | 24 | 17 | 9 | 6 | 318 |
| Bismark, North Dakota | 39 | 4 | 4 | 4 | 9 | 11 | 10 | 12 | 13 | 12 | 10 | 6 | 4 | 308 |

The National Bureau of Standards is carrying out tests in Hawaii between a 3 km mountain peak and a point at sea level 24 km distant. These tests are being made to further improve the accuracy to which a troposphere refractivity profile based on variables such as temperature, pressure, wind, and moisture content can be calculated. The Bureau of Standards hopes to compile another series of refractivity tables based on the new findings.

The Mitre Corporation is currently developing a "line integral refractometer" to provide a measure of refractivity based on only the moisture content (largest unknown in terms of radiowave refraction) and oxygen content of the troposphere (Reference 8).

Finally, the section entitled "Ionospheric Errors" includes some current thoughts regarding ionospheric effects above 100 Mc. It should be pointed out that azimuth angle measurement errors due to the atmosphere's departure from spherical stratification are not considered in this report. Measurements at Cape Kennedy demonstrate that for elevation angles above 5° there is generally a negligible effect on ray-bending due to tropospheric horizontal inhomogeneity (Reference 9). A horizontally inhomogeneous ionosphere will occur whenever a measurement ray passes from a daylight to nighttime region; however, the effect on azimuth angle measurement at frequencies above 1 kMc is negligible.

## TROPOSPHERIC ERRORS

### General

Figure 4 indicates the physical relationship between the troposphere and ionosphere above the earth's surface. The index of refraction, n, in the troposphere is given by

$$n = \frac{c}{V_p} = \sqrt{\epsilon_r \mu_r} , \qquad (1)$$

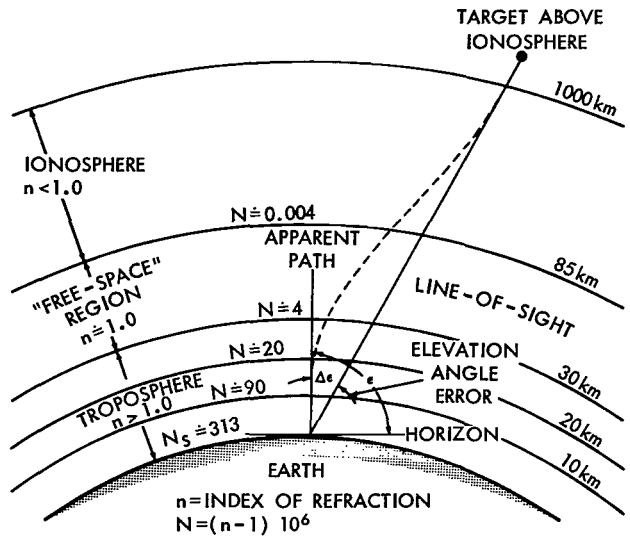


Figure 4—Relationship between *troposphere and ionosphere.*

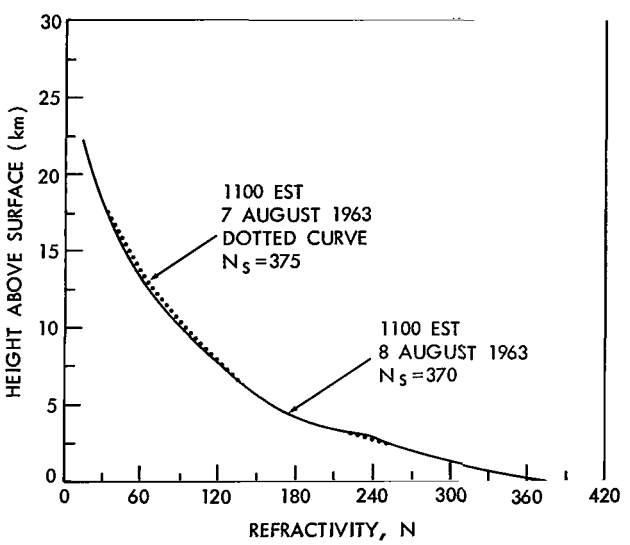


Figure 5—Measured tropospheric refractivity (data from Reference 5).

where

c = speed of light

$V_p$ = velocity of propagation in medium of index n

$\epsilon_r$ = relative dielectric constant of medium and

$\mu_r$ = relative permeability of medium.

For all practical purposes the relative permeability of the troposphere is that of freespace (i.e., $\mu_r = 1.0$) and therefore the dielectric constant at any point within the troposphere is a measure of the index of refraction at that point. This relationship between $\epsilon_r$ and n is sometimes used in measuring tropospheric index of refraction profiles by means of a microwave refractometer (Reference 9).

Another scheme for measuring the lower troposphere refraction profile is by means of an expendable balloon-borne radiosonde which transmits meteorological data back to earth from heights of 0 to 15 km. The radiosonde is automatically tracked by a high-gain antenna, thus assuring sufficient data for a continuous profile. Measured profiles for Valkaria, Florida, as obtained from this system (the "Rawin System") are shown in Figure 5. The two curves for 1100 hours EST 7 August 1963 and 1100 hours EST 8 August 1963 indicate the degree of variation one can expect in day-to-day measurements for the same time of day (i.e., no diurnal effect). The slight differences between the profiles are attributed to day-to-day changes in cloud cover.

Since the index of refraction, n, associated with the atmosphere is always near unity, it is general practice to describe this index in terms of the "refractivity," N, where

$$N \equiv (n - 1)\, 10^6 \,. \qquad (2)$$

This notation is useful when considering either the troposphere or the ionosphere.

The dielectric constant (and therefore N) of the troposphere is a function of temperature, total atmospheric pressure and water vapor pressure. The empirical relationship used for calculating N is given by the National Bureau of Standards (Reference 7) as

$$N = \frac{77.6}{T}\left(P + \frac{4810\, e_s\, RH}{T}\right), \tag{3}$$

where

$T$ = temperature in degrees Kelvin

$P$ = total atmospheric pressure (millibars)

$RH$ = % relative humidity

$e_s$ = saturation vapor pressure (millibars).

The constants in Equation 3 were determined from a consideration of recent microwave and optical determinations of the refractive index of air and the result is considered to be accurate to within 0.5% in N for frequencies up to 30 kMc in the ranges of temperature, pressure, and humidity normally encountered. Thus time delay and elevation angle errors due to tropospheric refraction are frequency independent in the 3 Mc to 30 kMc radio frequency range.

An exponential mathematical model for N within the troposphere has been introduced by the National Bureau of Standards. It is of the form

$$N = N_s \exp\left[-k(h - h_s)\right], \tag{4}$$

where

$N_s$ = refractivity at earth's surface

$k$ = decay constant (per km)

$h$ = height above surface corresponding to N (km)

$h_s$ = height of reference point above mean sea level (km).

The decay constant is generally calculated from a refractivity measurement at a height of 1 km. That is,

$$k = \ln \frac{N_s}{N_s + \Delta N}. \tag{5}$$

$N_s + \Delta N$ = refractivity at height of 1 km above surface (Reference 4). Equation 4 has been shown to accurately account for the mean tropospheric refraction of solar radio energy at

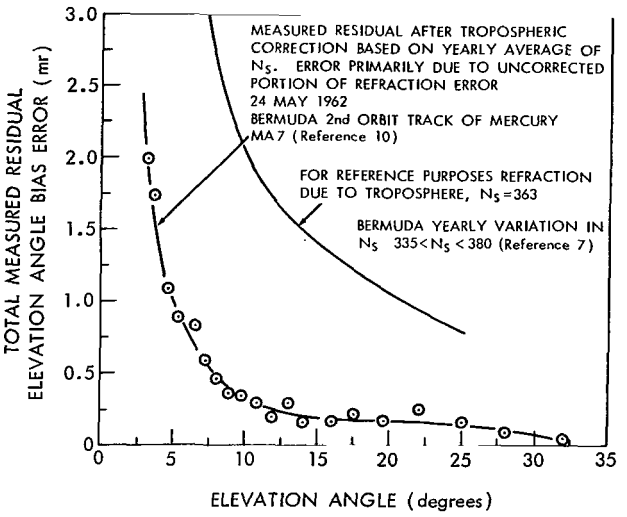


Figure 6—Total measured residual elevation angle bias for FPS/16 track of MA7. Tracking time from 1.7° elevation to 45.2° elevation is approximately 2 minutes.

16.2 kMc and 34.5 kMc, frequencies well above the range affected by the ionosphere. This measured data was presented previously in Figure 1.

The total measured residual elevation bias error at BDA, Bermuda, associated with an FPS/16 radar (5400-5900 Mc) track of the second orbit of Mercury MA7 is presented in Figure 6. While the method for obtaining the absolute calibration of this particular radar is not presented in Reference 10, it is of interest to note that there are no large deviations from the observed minus computed (o-c) angle error curve. At the time these data were taken, only yearly average values of surface refractivity were in use at the various tracking stations and the magnitude of the residual elevation error is not surprising. The measured residual of Figure 6 was obtained using the same computed orbit for each data point.

## Tropospheric Elevation Angle Error

The elevation angle error due to tropospheric refraction can be deduced from Snell's law for spherically stratified media. This law is given by

$$nr \cos \epsilon = n_0 r_0 \cos \epsilon_0 , \tag{6}$$

where

$n$ = index of refraction at lower layer

$n_0$ = index of refraction at upper layer

$r$ = radius to lower boundary associated with $n$

$r_0$ = radius associated with boundary of $n$ and $n_0$

$\epsilon$ and $\epsilon_0$ = ray local elevation angles.

The geometry is indicated by Figure 7. Equation 6 is used as the basis for the derivation of the classic expression for the bending of a radio ray (References 4 and 9), namely

$$\tau = - \int_1^2 \frac{dn}{n} \cot \epsilon_0 . \tag{7}$$

It can be shown (Reference 9) by integrating Equation 7 by parts that the bending through the total troposphere at elevation angles, $\epsilon$ (Figure 8), greater than 5°, the total refraction, $\tau$, is given to within 10% by

$$\tau = \left(N_s \cot \epsilon\right) 10^{-6} \text{ radians} , \tag{8}$$

where

$\tau$ = total refraction

$N_s$ = surface refractivity (10% accuracy for $\epsilon$ = 5°;

$\epsilon$ = ground elevation angle 2% accuracy for $\epsilon \geq 10°$).

The tropospheric refraction correction currently being employed in the Gemini program is an approximate evaluation of the integral of Equation 7. This approximation offers good agreement with the National Bureau of Standards ray-tracing tables for elevation angles greater than 2° and has the added advantage of being easy to implement into a computer program. This formulation was first presented by H. E. Clark of the Data Operations Branch, Goddard Space Flight Center, in 1963 (Reference 10). With reference to Figure 8,

$$\tau = \left[\left(N_s \times 10^{-6}\right)(\cot \epsilon)\right]\left[1.03585796 - \frac{1.072014 \times 10^{-2}}{\epsilon} + \frac{1.279119 \times 10^{-8}}{\epsilon^2} - \frac{1.227363 \times 10^{-8}}{\epsilon^3}\right] \quad 2° < \epsilon < 10° \tag{9}$$

$$\tau = \left(N_s \times 10^{-6}\right) \cot \epsilon \qquad 10° < \epsilon < 90° ,$$

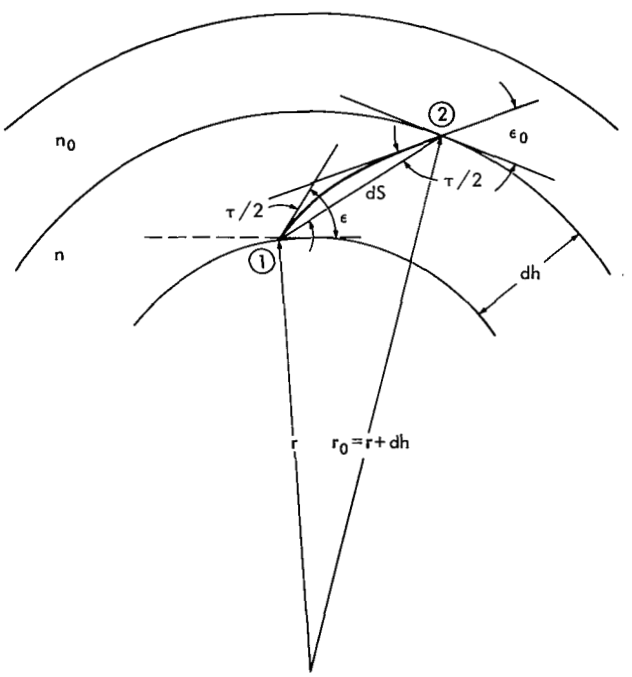


Figure 7—Ray bending geometry.

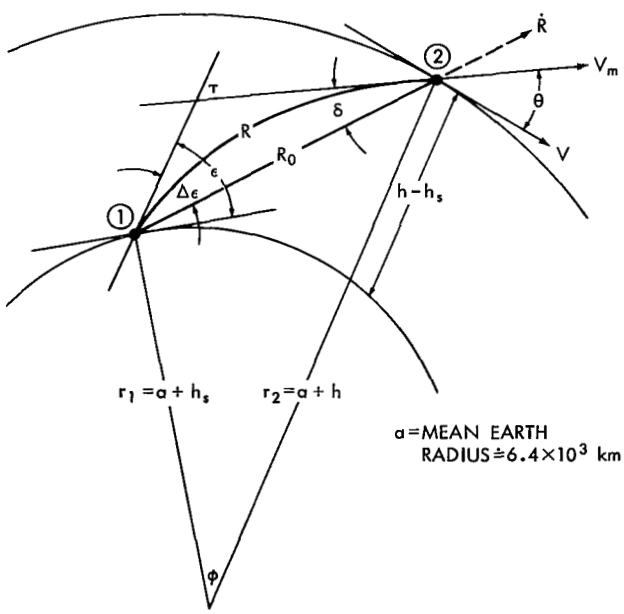


Figure 8—Troposphere ray-tracing geometry.

where

$\epsilon$ = observed elevation angle (radians)

$N_s$ = surface refractivity

$\tau$ = refraction (radians).

The present refraction corrections utilizing Equation 9 are based on the monthly average of surface refractivity for a particular site. Since the monthly change in surface refractivity for a particular time of day is a rather slow function of time (refer to Figure 3), any deviation from the monthly average is primarily due to the cyclic diurnal variations which, as shown by Table 1, will seldom exceed a change in N of ±10.

From the geometry of Figure 8, it is seen that the limits of the elevation angle error, $\Delta\epsilon$, in terms of the refraction, $\tau$, are given by

$$\frac{\tau}{2} \leq \Delta\epsilon \leq \tau \ .$$

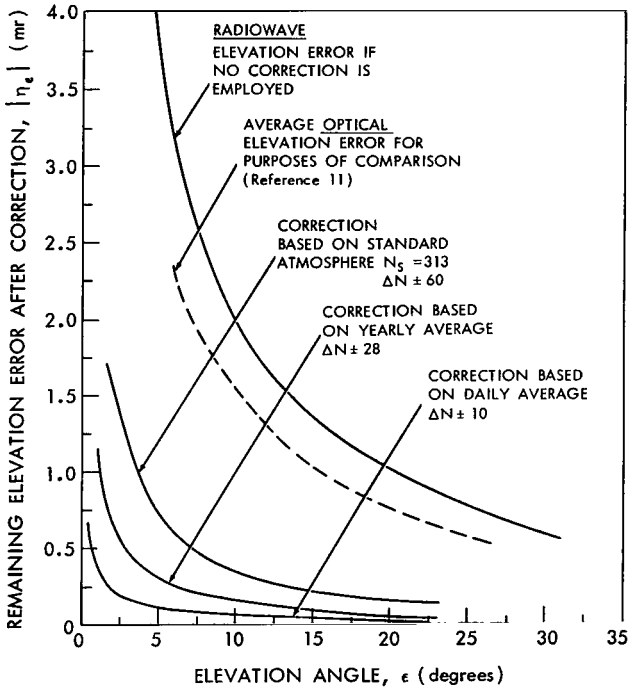


Figure 9—Elevation angle error due to tropospheric refraction. Vehicle height is 200 km. Maximum remaining error after correction is based upon exponential troposphere ray-tracing. Results are applicable to most tracking sites and in particular, those near Miami, Florida; Flagstaff, Arizona; Brownsville, Texas; Washington, D. C.; Fresno, California; Bismark, North Dakota; and Hamilton, Bermuda.

Furthermore, as the height, h, is increased without limit, $\Delta\epsilon$ approaches $\tau$. For all practical purposes, when considering heights above 200 km and elevation angles above 5°, $\tau = \Delta\epsilon$.

The NBS ray-tracing tables (Reference 4) present in tabular form the tropospheric elevation angle error, $|\Delta\epsilon|$, resulting from ray bending in an exponential atmosphere. The results are tabulated for each of 8 values of $N_s$ (i.e., $N_s$ = 200.0, 252.9, 289.0, 313.0, 344.5, 377.2, 404.8 and 450.0) with surface-to-target heights from 0 to 450 km. Since 450 km is well into the ionosphere (see Figure 4) the higher altitude calculations (as pointed out in the section entitled "Ionospheric Errors") will require modification for an estimate of total error. This is especially true if frequencies below 2 kMc are employed.

From the foregoing data the following figures have been derived: Figure 9 shows the maximum error, $|\eta_\epsilon|$, in elevation angle determination as a function of elevation angle for corrections based upon the standard atmosphere, best yearly average, and best daily average values of $N_s$.

The curve marked "no correction" represents a ray tracing using the National Bureau of Standards exponential model for a typical value of $N_s$ (373 in this case). An examination of the ray-tracing data (Reference 4) reveals that the refraction error for a given elevation angle is, for all practical purposes, a linear function of surface refractivity for the case of elevation angles greater than 2 degrees when target heights are greater than 200 km and surface refractivity is greater than 200. This means that at any given elevation angle an error in the determination of the surface refractivity will produce a certain error in elevation angle determination independent of the actual value of the surface refractivity. That is, the error after correction is only a function of the difference between the true value, $N_s$, and assumed value, $\bar{N}_s$.

As indicated in the introduction, the maximum diurnal variation is on the order of ±10 for the 7 sites listed in Table 1. Also, a value of ±28 was shown appropriate for maximum yearly variations in $N_s$. If a standard atmosphere of $N_s = 313$ is used, the uncertainty in $N_s$ at any given site can often be ±60. Figure 9 is therefore appropriate for most tracking sites. The data in Reference 9 indicate that the variations in yearly $N_s$ at Woomera, Australia, and Madrid, Spain, would be less than that experienced at the tracking sites in Florida and hence the results are somewhat pessimistic for these locations. Figure 9 is appropriate for estimating the tropospheric introduced elevation angle error for satellites or space vehicles at or above an altitude of 200 km. Figure 4, which relates the physical relationship between the troposphere and ionosphere, shows why total tropospheric ray bending is independent of altitude above 200 km. The value of N at 200 km is an inverse function of frequency squared and for sufficiently high frequencies can be taken as zero (i.e., freespace).

## Tropospheric Range Error

The tropospheric range measurement error between a target and the earth's surface is primarily due to the electrical path length difference between a line-of-sight path measured in terms of the velocity of light in vacuum and the line-of-sight electrical path length due to the actual velocity of propagation associated with the troposphere. A second-order effect is the physical path length difference between the ray path and the line-of-sight path. The National Bureau of Standards ray tracings include both factors. A certain degree of insight regarding the major source of tropospheric range error can be obtained from the following derivation which gives a range error approximation (97% of total error for $\epsilon > 10°$) due only to electrical path length difference.

The path length between ground station and target (points 1 and 2, Figure 8) is given by

$$R_0 = \int_1^2 ds = \text{line-of-sight range} . \tag{10}$$

The "apparent range" due to a velocity of propagation less than that of light in vacuum is given by

$$R = \int_1^2 nds = \text{apparent range} . \tag{11}$$

The difference between Equation 10 and 11 is the one-way range error, $\Delta R$, or

$$\Delta R = \int_1^2 (n-1)\, ds \; ; \tag{12}$$

but

$$(n-1) \cong N\left(10^{-6}\right)$$

and Equation 12 becomes

$$\Delta R = \int_1^2 N\left(10^{-6}\right) ds \; . \tag{13}$$

But from the geometry of Figure 7 it is seen that

$$ds = \frac{dh}{\sin \epsilon} = dh \csc \epsilon \; . \tag{14}$$

Combining Equations 13 and 14

$$\Delta R = 10^{-6} \int_1^2 N \csc \epsilon \, dh \; . \tag{15}$$

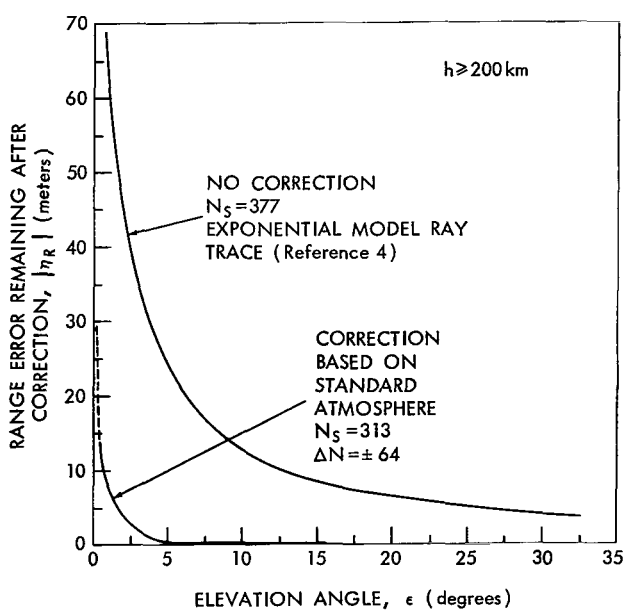


Figure 10—Tropospheric range error remaining after correction versus elevation angle. The error remaining after correction represents the difference between ray-traces at $N_s$ = 377 and $N_s$ = 313 (standard atmosphere).

Equation 15 indicates that the range error, like the elevation angle error, is a function of the refractivity profile. It can be shown (Reference 9) that Equation 15 can, for elevation angles $\epsilon > 10°$, be approximated by

$$\Delta R \doteq \csc \epsilon \left(10^{-6}\right) \int_{h_1}^{h_2} N \, dh \; , \tag{16}$$

where

$h_1$ = height of surface above sea level,

$h_2$ = target height,

which for $\epsilon > 10°$ accounts for 97% of the range error. Figure 10 indicates the range error remaining after correction with a correction based only upon the often accepted standard value of $N_s$ = 313.0. It is apparent that for elevation angles greater than 5°, the range

correction is not a critical function of $N_s$ since, as shown by Figure 10, the remaining error after correction is only 0.5 meters at 5° even though the ray-tracing is for a difference of ±64 between the true and assumed values of N. The insensitivity in range error to surface refractivity when the entire troposphere is traversed (h > 85 km) is due to the fact that the absolute value of the decay constant, k, of Equation 4 is observed in nature to be inversely related to the surface refractivity, $N_s$. Thus the integrated time delay experienced in tracing a ray through the entire troposphere is to a certain extent invariant with changes in surface refractivity.

The tropospheric error indicated is appropriate for lunar distances as well as earth orbits. It should be pointed out that at lunar distances the limit on range accuracy is the accuracy to which the velocity of light is known. An estimate of the range and angle non-systematic or noise errors due to tropospheric anomalies in cloud cover is indicated in Table 2 (Reference 12). The noise errors indicated in Table 2 are pessimistic in that short term fluctuations are smoothed by the overall time response of the tracking system. That is, the system discerns the mean value of $N_s$ as indicated by the measured data of Figure 6.

Table 2

Estimated Range and Angle Noise Due to Troposphere.

| Type of Weather | Refractivity Fluctuation, ΔN RMS | 5 Degree Elevation | | 20 Degree Elevation | |
|---|---|---|---|---|---|
| | | Elevation Fluctuation, $\delta_\epsilon$ RMS (mr) | Range Fluctuation, $\delta_R$ RMS (meters) | Elevation Fluctuation, $\delta_\epsilon$ RMS (mr) | Range Fluctuation, $\delta_R$ RMS (meters) |
| Heavy Cumulus | 30 | 0.4 | 0.5 | 0.2 | 0.25 |
| Scattered Cumulus | 10 | 0.2 | 0.12 | 0.1 | 0.06 |
| Small Scattered Cumulus | 3 | 0.1 | 0.02 | 0.05 | 0.01 |
| Clear Moist Air | 1 | 0.04 | 0.005 | 0.02 | 0.0025 |
| Clear Normal Air | 0.3 | 0.02 | 0.001 | 0.01 | 0.0005 |
| Clear Dry Air | 0.1 | 0.01 | 0.0002 | 0.005 | 0.0001 |

## Tropospheric Range-Rate Error

The errors in range-rate measurement due to signal passage through the troposphere can be attributed to the following causes:

1. The angular difference between the refracted ray at the vehicle and the ground to vehicle line-of-sight.

2. Incorrect assumptions regarding the magnitude of the refractive index at the space vehicle.

3. Changes in index of refraction profile during the Doppler frequency measurement interval introducing an error when integrated Doppler is averaged over a finite time (usually one second or greater).

4. Short term fluctuations in the index of refraction associated with the vehicle-to-ground radio path. Such "noise" fluctuations include those due to clouds, rain, and changes in propagation path as the vehicle passes through various strata at a constant radio distance from the ground station.

Since this paper is concerned with vehicles at altitudes above 200 km, the vehicle will be well above the troposphere (see for example, Figure 4) and consequently, the first two error sources, angular error and local vehicle refractive index errors, are attributed to the ionosphere and are discussed under "Ionospheric Range-Rate Error." The tropospheric range-rate errors generally considered in the literature are those assuming "instantaneous Doppler frequency" measurements in which case range-rate error for a target traversing the atmosphere is considered as only the localized error at the specific point in the medium associated with the space vehicle. From this viewpoint, the troposphere acts merely as a refraction medium (Reference 13). In practice, however, the Doppler shift associated with a satellite pass of space vehicle motion is obtained by counting Doppler cycles of phase change over a finite time interval (often 1 second) and obtaining the average Doppler rate for this interval. With this practical consideration in mind, it is noted that the range-rate error due to a different index of refraction profile at the beginning and end of the sampling period will be equal to the difference between the range errors associated with the beginning and end of the measurement interval divided by the time interval of the measurement.

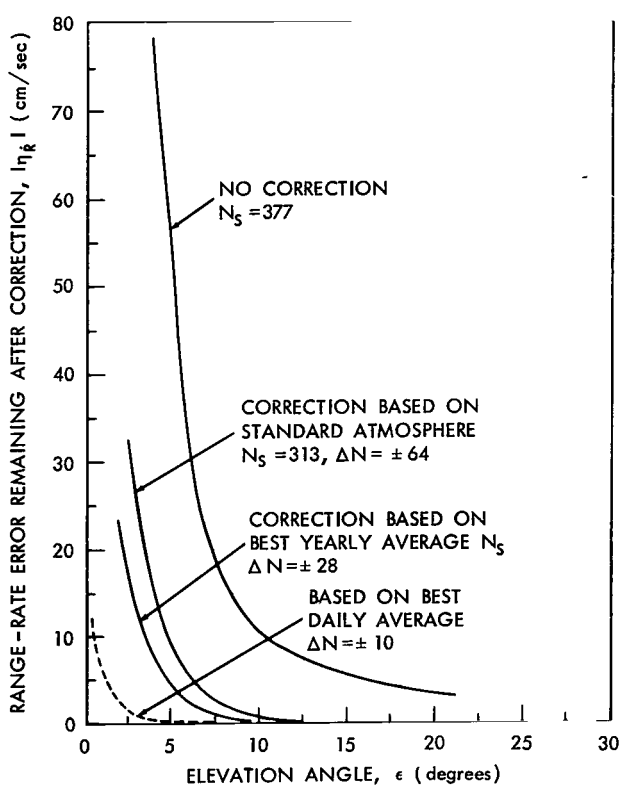


Figure 11—Range-rate error due to troposphere (altitude, 225 km; circular earth overhead orbit vehicle speed, 7.85 km/sec; error decreases for higher altitudes).

Figure 11 shows the remaining range-rate error, $|\eta_{\dot{R}}|$, as a function of elevation angle after a standard atmosphere ($N_s$ = 313) correction, after a correction based on a best yearly average, and after correction based on the best daily average of $N_s$. This curve is for a 200 km overhead earth parking orbit. The tropospheric range-rate error was derived from NBS ray-tracing data (Reference 4) in the following manner.

The tropospheric range error versus elevation angle curves for $N_s$ = 377, $N_s$ = 367,

$N_s = 349$, and $N_s = 313$ were graphically differentiated to obtain curves of the rate of change of range error with respect to elevation angle, $d(\Delta R)/d\epsilon$, versus elevation angle, $\epsilon$.

Also a curve of earth central angle $\phi$, (Figure 8) versus elevation angle, $\epsilon$, was obtained from the ray tracing data of Reference 4. It was noted that in the range $1° < \epsilon < 12°$ $\epsilon$ is linearly approximated by

$$\epsilon \doteq -1.55\phi + 0.46 \text{ radians} , \tag{17}$$

where

$\epsilon$ = elevation angle (radians)

$\phi$ = central angle (radians).

And since the vehicle speed is 7.85 km/sec (nominal Apollo earth parking orbit speed), the angular velocity $d\phi/dt$, is given by

$$\frac{d\phi}{dt} = \frac{V}{r} = 1.19 \times 10^{-3} \text{ radians/second} , \tag{18}$$

where

V = vehicle speed = 7.85 km/sec

r = earth radius plus altitude of vehicle = 6378 + 225 = 6603 km.

Combining Equations 17 and 18 it is noted that the elevation angular velocity is simply

$$\frac{d\epsilon}{dt} = (-1.55)\frac{d\phi}{dt} = -1.85 \times 10^{-3} \text{ radians/second} \qquad 1° \leq \epsilon \leq 12° . \tag{19}$$

The change in range per unit time can then be obtained as

$$\frac{\Delta R_1 - \Delta R_2}{\Delta T} = \left(\frac{d(\Delta R)}{d\epsilon}\right)\left(\frac{d\epsilon}{dt}\right) = \left(\frac{d(\Delta R)}{d\epsilon}\right)\left(-1.85 \times 10^{-3} \text{ radians/second}\right) , \tag{20}$$

where

$d\epsilon/dt$ = elevation angle rate of change (radians/second)

$\Delta R_1$ = range delay error at $\epsilon_1$ (meters)

$\Delta R_2$ = range delay error at $\epsilon_2$ (meters)

$\Delta T$ = time period of integration (seconds)

$d(\Delta R)/d\epsilon$ = rate of change of range error with respect to elevation angle obtained from graphical differentiation of ray-tracing range error versus elevation angle curve.

Equation 20 is plotted for $N_s = 377$ in Figure 11. For every elevation angle, the change in range error in cm over a one second interval represents the range-rate error in cm/sec. It is seen that this range-rate error is independent of the averaging time, $\Delta T$, as long as the slope of range error versus elevation angle, $d(\Delta R)/d\epsilon$, does not change appreciably during the measurement interval. This condition is met for a sampling rate $\Delta T$ up to minutes depending on vehicle angular velocity relative to the tracking station.

In the Apollo Mission the lunar parking orbit is to be maintained at a nominal height of 185 km above the moon's surface at a speed of 2.28 km/sec (Reference 14). The range-rate error versus elevation angle curve shown in Figure 11 is not appropriate for lunar orbits since it is based on earth orbit geometry and velocity. With reference to Figure 12 it is seen that the angular rate of change of the vehicle relative to earth central angle $\phi$ (assuming a stationary earth) is quite slow and is given approximately by

$$\frac{d\phi}{dt} \doteq \frac{V}{R_0} = 6 \times 10^{-6} \text{ radians/second} , \tag{21}$$

where

$V$ = lunar orbit linear speed = 2.28 km/sec

$R_0$ = earth-moon mean distance = $3.84 \times 10^5$ km.

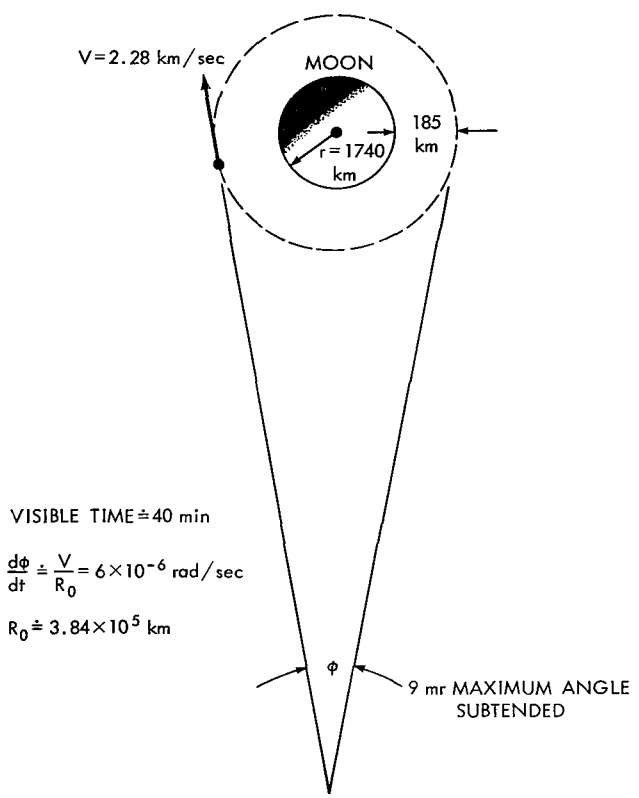


Figure 12—Lunar orbit geometry (Apollo lunar parking data from Reference 14).

Therefore at lunar distance and beyond, the maximum range-rate error is due solely to the earth's rotation, which is on the order of $7 \times 10^{-5}$ radian per second. The uncorrected range-rate error at lunar distances for $N_s = 377$ is shown in Figure 13.

A verification of the foregoing analysis is presented by Figure 14, which shows the estimated residual two-way Doppler at 960 Mc from Ranger VI (Reference 15) at a distance where only earth rotation is important. The range-rate error corresponding to the two-way Doppler is given by

$$\frac{dR}{dt} = \frac{d\phi}{dt}\left(\frac{\lambda}{4\pi}\right) = f_d\left(\frac{\lambda}{2}\right) = 15.6\, f_d \text{ cm/sec} , \tag{22}$$

where

$f_d$ = two-way Doppler rate (cps).

The calculated range-rate error of Figure 13 due to the earth's rotation is given by Equation 20 for the case $d\epsilon/dt \doteq -7 \times 10^{-5}$ radian/second.

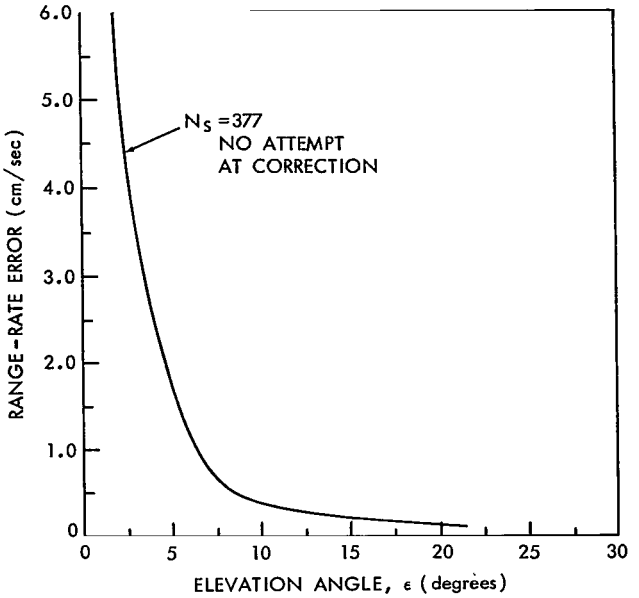


Figure 13—Range-rate error due to troposphere and earth rotation.

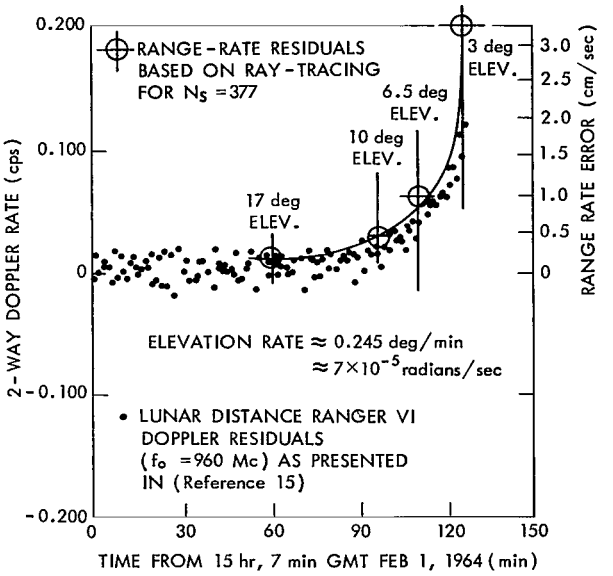


Figure 14—JPL Doppler correction compared to correction based upon ray-tracing (elevation rate ≈ 0.245 deg/min ≐ $7 \times 10^{-5}$ radians/sec).

It is seen that Figure 13, when replotted in Figure 14, fits the Jet Propulsion Laboratory data quite well. The Jet Propulsion Laboratory uses an empirical correction for the tropospheric refraction effect upon range-rate data. The JPL data in Figure 14 were obtained by generating best fit orbit data and then comparing these data to those obtained without the refraction correction terms. It appears that the ray-tracing range-rate refraction correction derived in this paper is appropriate for sampling times at least up to one minute, the sampling rate associated with Ranger VI in Figure 14. It is seen that rather straightforward correction terms can be obtained from the derivatives of the ray-traced range error curves for either earth orbit or lunar distance space travel. At the particular frequency of 960 Mc used on Ranger VI, the total range-rate error due to the atmosphere can be accounted for by the troposphere.

An estimate of tropospheric short term Doppler error (noise) based on range fluctuations measurements by NBS is presented in Table 3 (Reference 16).

The noise estimate is seen to be considerably less than the biasing error due to tropospheric effects and is generally independent of elevation angle. The reason for this is illustrated by the equation describing the Doppler signal as received at the ground station. Under "Tropospheric Range Error," it

Table 3

RMS Range-Rate Noise Due to Tropospheric Fluctuations (1-Way Transmission).

| Doppler Integration Time (seconds) | Cloud Coverage | | |
|---|---|---|---|
| | Small | Average | Large |
| | $\dot{R}$ Noise (cm/sec) | | |
| 1.0 | 0.016 | 0.022 | 0.075 |
| 5.0 | 0.015 | 0.020 | 0.055 |
| 20.0 | 0.010 | 0.015 | 0.030 |
| 60.0 | 0.003 | 0.009 | 0.020 |

was shown that the apparent range, R, is given by

$$R = \int_1^2 n\,ds = \int_{s_1(t)}^{s_2(t)} n(t, s)\,ds , \tag{23}$$

where

$n(t, s)$ = tropospheric index of refraction along path of integration, a function of time and path

$s_2$ = ray terminating point at vehicle

$s_1$ = ray terminating point at earth = 0 or reference of coordinate system used in performing the integration and the geometry is as indicated by Figure 8.

But the range rate $dR/dt = \dot{R}$ is given by

$$\dot{R} = \frac{\partial}{\partial t} \int_{s_1(t)=0}^{s_2(t)} n(t, s)\,ds = \int_0^{s_2} \left(\frac{\partial n}{\partial t}\right) ds - n_1 \frac{ds_1}{dt} + n_2 \frac{ds_2}{dt}$$

or

$$\dot{R} = \int_0^{s_2} \left(\frac{\partial n}{\partial t}\right) ds + n_2 \frac{ds_2}{dt} . \tag{24}$$

The first term in Equation 24 relates the measured "apparent change in range rate" due to the fluctuations in index of refraction, $n$, along the ray path between points 1 and 2. The short term fluctuations are generally due to cloud cover and hence not a critical function of elevation angle $\epsilon$. The first term includes the change in $n$ during Doppler averaging. The second term is a function of the range rate $ds_2/dt$, which is the velocity of the vehicle projected upon the tangent of the ray path at the vehicle, and the index of refraction at the vehicle. The second term is entirely a function of the medium characteristics at the vehicle and for a vehicle height of 200 km is concerned with the ionosphere.

## IONOSPHERIC ERRORS

### General

Correction procedures based on use of ionospheric profiles have not proved very accurate to date (1965) and may not lead to any significant reduction of error. The estimates of error reduction run from negligible to a factor of four (i.e., leaving 25% of the initial error). The improvement realized is quite dependent upon the stability of that portion of the ionosphere through which the measurement ray passes. The ionospheric layers are always in a state of motion near dusk or

dawn (Reference 12). It is therefore desirable to obtain an estimate of the maximum daytime or nighttime ionospheric error which could be experienced at any given frequency and consider this value as the limiting uncorrectable error due to ionospheric effects.

The index of refraction at a given point within ionized media such as the ionosphere is defined as the ratio of the velocity of light in vacuum, $c$, to the phase velocity, $V_p$, or

$$n = \frac{c}{V_p} = \left(1 - \frac{N_e e^2}{\epsilon_0 m \omega^2}\right)^{1/2}, \qquad \text{(Reference 17)} \qquad (25)$$

where

$V_p$ = phase velocity

$c$ = speed of light in vacuum

$N_e$ = electron density = electrons/meter$^3$

$e$ = electron charge = $1.602 \times 10^{-19}$ coulombs

$m$ = electron mass = $9.11 \times 10^{-31}$ kilograms

$\epsilon_0$ = free space dielectric constant = $8.855 \times 10^{-12}$ farad/meter.

This definition of index of refraction is consistent with that presented in Equation 1 for non-conducting media where "velocity of propagation" is equal to "phase velocity." In order to properly interpret Equation 25 the concept of phase and group velocity must be briefly reviewed.

Phase velocity is that velocity one must travel to keep the instantaneous phase constant; that is, if $e^{j(\omega t - \beta z)}$ represents the phase factor associated with a sinusoidal continuous signal where

$\omega$ = angular frequency = $2\pi f$

$f$ = frequency of oscillation

$\beta$ = phase delay per unit distance = $\omega/V_p$

$V_p$ = phase velocity

$z$ = distance between source and observer,

then it is noted that the instantaneous phase $(\omega t - \beta z)$ does remain constant if one travels with velocity $V_p$ such that $z = V_p t + K$, where $K \equiv$ a constant.

In nondispersive media (i.e., where the phase velocity is not a function of frequency) such as the troposphere the "phase velocity" and "velocity of propagation" (or more precisely signaling velocity) are identical. This is not so in the ionosphere as might be deduced from Equation 25 which indicates $|V_p| > c$.

Signal velocity is associated with the velocity of propagation of the envelope of a modulated sinusoid.. The modulation in the case of a ranging system is often simply a pulse or series of

pulses. Since a modulated sinusoid will consist of a spectrum of frequencies, phase distortion is inherent in dispersive media. However, if the transmitted spectrum is narrow compared with the carrier frequency, an average "signal or group velocity" can be calculated which can be used to calculate time delays through the ionosphere. This velocity is given by (Reference 18)

$$V_g = \frac{V_p}{1 - \frac{\omega}{V_p}\left(\frac{dV_p}{d\omega}\right)} \quad . \tag{26}$$

Differentiating Equation 25 and substitution into Equation 26 yield, after some manipulation,

$$V_g = V_p n^2 = nc \quad , \tag{27}$$

for

$$n \leq 1 \quad .$$

That is, since $n < 1$, the group velocity in the ionosphere is less than the velocity of light in vacuum and hence a time delay in signaling is realized.

## Ionospheric Elevation Angle Error

In principle, the ray-bending or refraction mechanism within the ionosphere is analogous to that of the troposphere. The measurement ray traverses a region of varying refractivity which is a function of electron density and excitation frequency as indicated by Equation 25. For this reason, ray-tracing techniques can be employed to obtain estimates of ionospheric refraction error. Figure 15 indicates the nature of the combined troposphere and ionosphere refraction geometry. The details of the overall ray path are related to the overall refractivity profile. At present only the troposphere refractivity profile is known with sufficient accuracy to permit real time bias adjustments of radar data. Models based on average daytime and nighttime ionosphere electron density profiles, however, are useful in estimating average biasing effects which can be attributed to the ionosphere. Separate

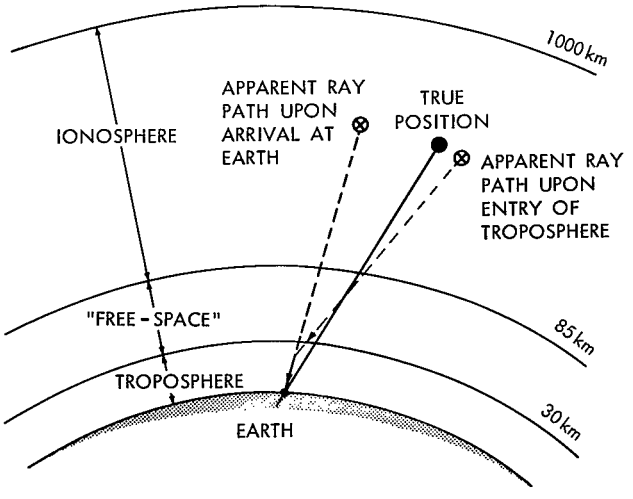


Figure 15—Tropospheric and ionospheric ray refraction.

ionospheric models are generally used for day and night since daytime ionization is considerably greater than nighttime ionization.

The value of refractivity, N, for the ionosphere is given by (Reference 16)

$$N = \left( \frac{-40.3 N_e}{f^2} 10^6 \right) , \tag{28}$$

where

$N_e$ = electron density (electrons/meter$^3$)

$f$ = frequency (cycles per second)

and

$$N \equiv (n - 1) 10^6 .$$

An example of a typical ionospheric refractivity profile at 2 kMc based upon data measured at Washington, D. C., is shown in Figure 16. These curves were originally presented in Reference 19 for 400 Mc and have been adjusted to 2 kMc by means of Equation 28. The maximum value of $N = -12$ corresponds to the maximum value of electron density $N_e = 1.2 \times 10^{12}$ electrons per cubic meter at an altitude of 300 km. A value of $10^{12}$ electrons/meter$^3$ for $N_e$ is seldom exceeded in the earth's ionosphere; hence a value of $N = -12$ is the maximum one might expect during any ionospheric ray tracing at 2 kMc. This is in contrast to the values of tropospheric N at the earth's surface which range from 300 to 400. The course and fine structure of the ionosphere is a subject of continuing measurement. Techniques for such investigation by means of satellite signal observation are presented in References 20 and 21.

As in the case of tropospheric refraction the maximum error in elevation angle occurs at low elevations. Also, maximum refraction is associated with maximum ionization and hence daytime ionospheric states. Figure 17, which is for 5° elevation and a daytime average ionosphere, thus relates the maximum mean elevation bias error as a function of frequency and altitude above the earth's surface. This analysis is based on a rectangular model of the ionosphere and was first presented by Pfister and Keneshea (Reference 22). Figure 18 indicates the rectangular electron density versus altitude approximation used to obtain ionospheric error estimates. While such a model is useful in estimating maximum error, it is apparent that it cannot be used for purposes of radar calibration.

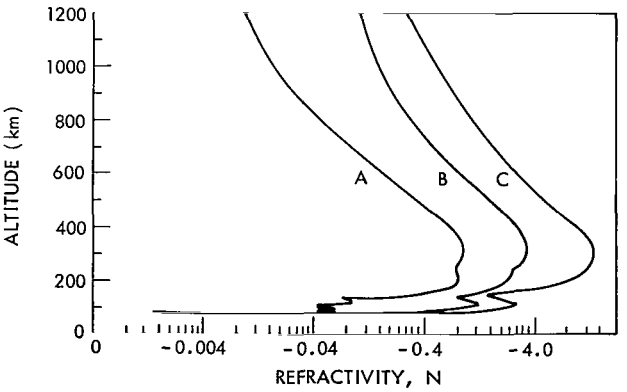


Figure 16—Ionospheric refractivity profiles at 2 kMc. Curves are reproduced from Reference 19 with a scale change according to Equation 28 to indicate the range of refractivity at 2 kMc. Profile A exceeded 97.5% of the time, B, 50% of the time and C, 2.5% of the time. Maximum electron density $\doteq 10^{12}$ electrons/m$^3$.

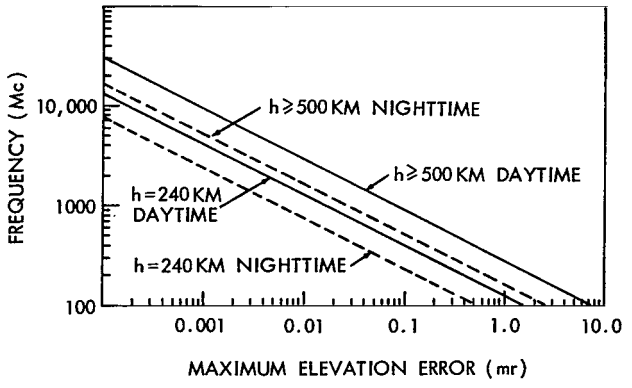


Figure 17—Ionospheric maximum elevation angle error for 5° elevation (from Reference 22). Error decreases as elevation angle increases above 5°.

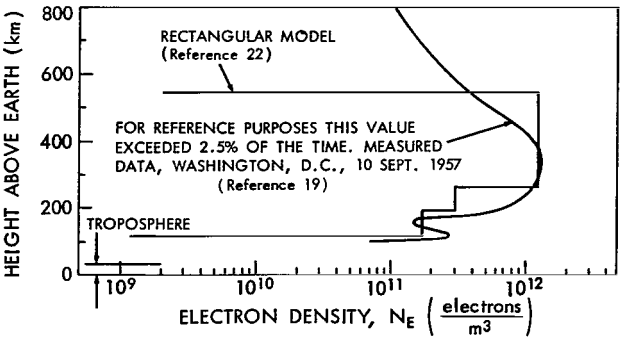


Figure 18—Daytime ionospheric model.

A number of measurements carried out on the California coast indicated that the ionospheric errors could not be predicted on the basis of ionograms (ionospheric soundings to obtain current profile data) any better than by using average monthly forecasts of electron density profiles and that the residual errors after attempted correction were almost as great as the original error values. The inability to predict the error encountered at a given time indicates that accurate systems must operate at frequencies high enough to reduce the initial values of ionospheric error to a tolerable value (Reference 1).

## Ionospheric Range Error

The range bias due to increased time delay relative to freespace delay of the signal through the ionosphere can be calculated only if the ionospheric index of refraction profile is accurately known. If only an average profile is known, the residual error can be estimated. The delay in an ionized media must be calculated using the group or signaling velocity indicated on page 20. The ionospheric range error due to time delay can then be calculated in a way analogous to the tropospheric development on pages 11 and 12;

$$R_0 = \int_1^2 ds = \text{line-of-sight range.} \tag{29}$$

The "apparent range" due to a phase velocity greater than that of light in vacuum is given by

$$R = \int_1^2 \frac{ds}{n} = \text{measured range,} \tag{30}$$

where

n = ionosphere index of refraction.

Equation 30 describes the apparent increase in range due to a group velocity less than the speed of light. Combining Equations 29 and 30, range error $\Delta R$ is given by

$$\Delta R = R - R_0 = \int_1^2 \left(\frac{1-n}{n}\right) ds \; ; \tag{31}$$

but $n = 1 + N \times 10^{-6}$ and Equation 31 can be written as

$$\Delta R = -10^{-6} \int_1^2 \frac{N\,ds}{1 + N \times 10^{-6}} \doteq -10^{-6} \int_1^2 N\,ds \; , \tag{32}$$

where, for the ionosphere,

$$N = -\left(\frac{40.3\,N_e}{f^2}\right) 10^6 \; ,$$

$N_e$ = electron density (electrons/meter$^3$),

$f$ = frequency (cps).

Figure 19, which is for 5° elevation and a daytime average ionosphere (a worst case situation), shows the maximum mean range bias error as a function of frequency and altitude.

Figure 20 shows the maximum ionospheric range error which can be expected at the Apollo

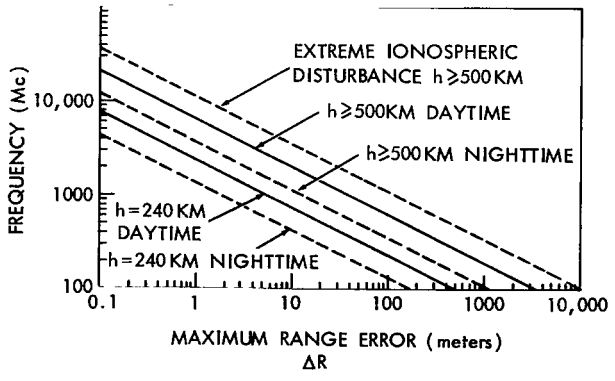


Figure 19—Ionospheric maximum range error for 5° elevation (from Reference 22). Error decreases as elevation angle increases above 5°.

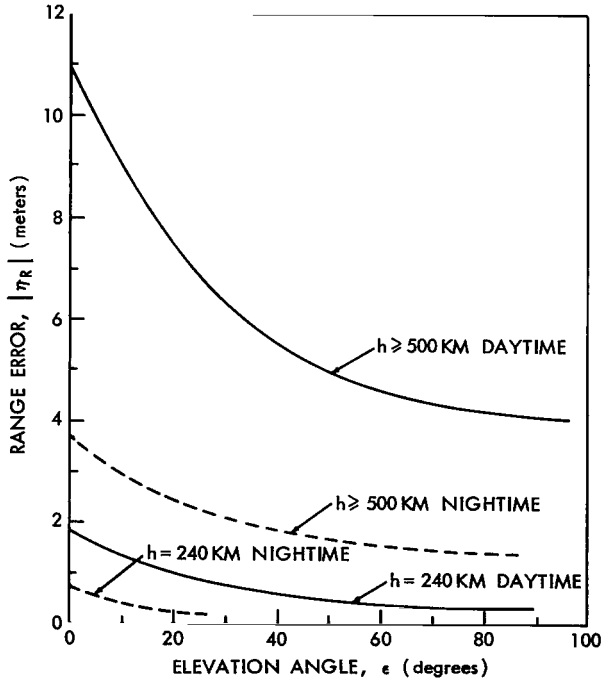


Figure 20—Ionospheric maximum range error at 2 kMc (from Reference 22).

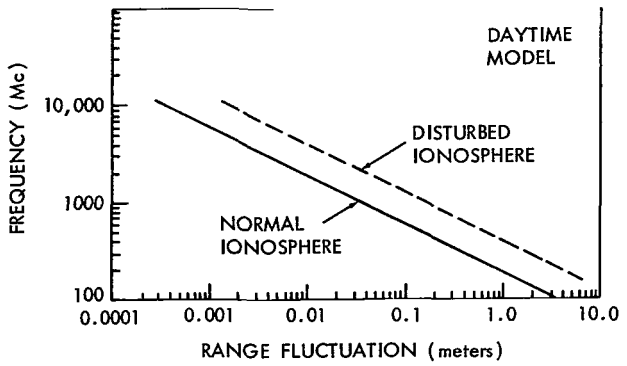


Figure 21—Ionospheric range fluctuation versus frequency for a 10° elevation angle.

Unified S-band frequencies (nominal 2 kMc) versus elevation angle. This figure is derived from the rectangular ionospheric refractivity profile analysis presented in References 16 and 22.

Figure 21 shows an estimate of ionospheric range fluctuation or noise as a function of frequency for a vehicle height of 240 km and 10° elevation (Reference 16).

## Ionospheric Range-Rate Error

It was shown on page 18 that the range-rate error can be separated into two parts, that is, the error due to time variations of the index of refraction, $n$, along the propagation path during the Doppler measurement interval and the localized error at the vehicle. In the case of a target traversing the ionosphere only the localized error is significant in the calculation of ionospheric error contribution (Reference 13). The value of the ionospheric index of refraction at the vehicle, $n_t$, can only be estimated and presents one limitation on overall Doppler error determination. The major ionospheric error source is due to the slight difference in direction of the refracted ray at the target and the ground to target line-of-sight.

The geometry of Figure 8 indicates a target velocity, $V$, the radial component along the line-of-sight, $\dot{R}$, and the apparent or measured radial component, $V_m$. The magnitudes of the Doppler of $\dot{R}$ and $V_m$ are given by

$$\dot{R} = V \cos(\theta + \delta) \tag{33}$$

$$V_m = V \cos\theta \ . \tag{34}$$

The magnitude of the error in measuring $\dot{R}$ is then given by

$$\Delta V_R = \dot{R} - V_m = V\left[\cos(\theta + \delta) - \cos\theta\right] \ . \tag{35}$$

But $\cos(\theta + \delta) = \cos\theta \cos\delta - \sin\theta \sin\delta$ and the angle $\delta$ is in all practical situations quite small such that Equation 35 can be approximated by

$$\Delta V_R \doteq -V\delta \sin\theta \ . \tag{36}$$

That is, the magnitude of the range-rate error is proportional to the target velocity, $V$, the angle between the refracted ray at the target and line-of-sight, $\delta$, and the sine of the local elevation angle, $\theta$.

Figure 22 shows an estimate of ionospheric range-rate bias as obtained by considering an average ionospheric profile and Equation 36. The radial velocity error is for Apollo earth orbit speeds (7.85 km/sec). The calculation is based on a height of 300 km which is the region of maximum ionization (hence maximum bending), as indicated by Figure 16. Therefore Figure 22 can be used to estimate the maximum ionospheric residual range-rate bias for earth orbiting vehicles traveling at a speed of approximately 8 km/sec. At lunar distances the lack of lunar atmosphere results in $\delta \to 0$ in Equation 12 and hence no significant error is contributed by the ionosphere.

Figure 23 depicts the maximum range-rate error attributable to the ionosphere as a function of elevation angle for the Nominal Unified S-band System (USBS) frequency of 2 kMc.

The range-rate bias due to a change in ionospheric range error over the range-rate measurement interval can be shown to be small relative to the same effect attributed to the troposphere. The reason for this is that the range delay experienced by a signal traversing the ionosphere is not a critical function of elevation angle. For example, at 1 kMc, at a height of 200 km or greater, and for a daytime ionosphere, the maximum rate of change of range error versus elevation angle is approximately 6 meters per radian, nearly independent of elevation angle (Reference 22). For a 225 km earth orbit and a velocity of 7.85 km/sec, this corresponds to a bias of 1 cm per second at elevation angles between 4° and 12°. It is noted that the tropospheric bias at 5° elevation due to the same phenomena is 50 cm per second (Figure 11). However, if range-rate data for vehicles within the ionosphere ever need to be corrected to within 1 cm per second, it is apparent this component of error is not negligible. At a frequency of 1 kMc or higher the tropospheric range-rate error will predominate by a factor of 5 or more for elevation angles up to 15°. In any case, at 1 kMc or above, this particular ionospheric range-rate biasing effect is less than that which can be attributed to the troposphere.

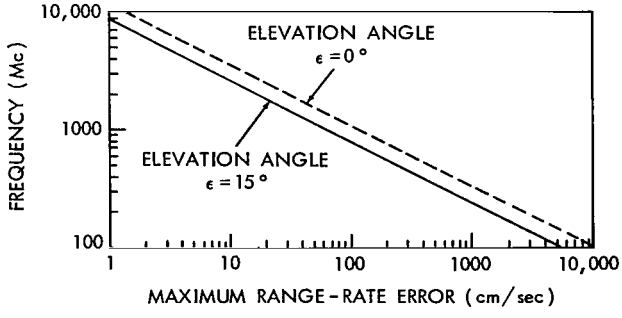


Figure 22—Ionospheric maximum range-rate error (from Reference 13) daytime ionosphere; error due to refraction at vehicle.

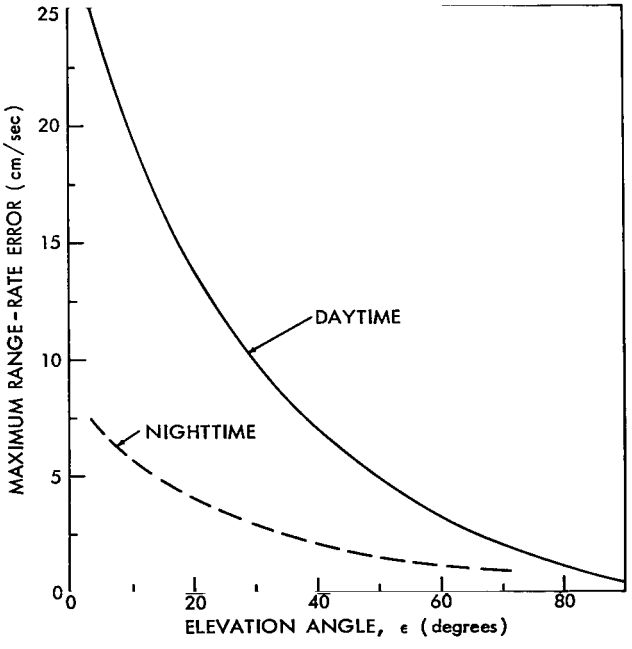


Figure 23—Ionospheric maximum range-rate error at 2 kMc; overhead earth parking orbit, h = 300 km, error due to refraction at vehicle (from Reference 13).

## CONCLUSIONS

The following is a two-part summary of this report. The first part consists of general statements concerning the influence of the atmosphere on microwave propagation between the earth's surface and a space vehicle located at or above an altitude of 200 km. This portion of the discussion examines separately the effect of the atmosphere upon measurements of elevation angle, range and range rate. The second part of this discussion summarizes the influence of the atmosphere upon radiowave propagation again for heights greater than or equal to 200 km but at the particular nominal radio frequency of 2 kMc. This frequency is of interest in that it approximates the operating frequency employed in the Unified S-Band System of the Apollo Program.

### Atmospheric Induced Error for Vehicle Heights Above 200 km

*Elevation Angle*

Elevation angle bias due to the atmosphere decreases with increasing elevation angle. Tropospheric refraction is generally frequency independent whereas ionospheric refraction is inversely proportional to frequency squared. Maximum uncertainty in angle of arrival determination occurs for vehicles at low elevations at points outside of the earth's atmosphere. With no attempt at correction, the maximum elevation angle bias will be on the order of 4 mr at 5° elevation independent of frequency for frequencies above 1 kMc (Figures 9 and 17). With a tropospheric refraction correction based on the best daily average of surface refractivity, the tropospheric bias at 5° elevation will be on the order of 0.1 mr (Figure 9). A 0.1 mr bias at 5° elevation attributable to the ionosphere can occur during the daytime at a frequency at or below 900 Mc (Figure 17). The nighttime maximum bias effect due to the ionosphere is about one third that experienced at daytime.

Elevation angle short-term fluctuations (period of fluctuation up to 10 minutes) also decrease with increasing elevation angle and for the troposphere are a function primarily of cloud cover. At frequencies above 1 kMc, the short-term fluctuations are associated primarily with the troposphere and estimates range from 0.4 mr RMS for heavy cumulus cover to 0.01 mr RMS for clear dry air. At 20° elevations, the corresponding estimates are 0.2 mr RMS and 0.005 mr RMS (Table 2).

*Range*

Range biasing effects due to the atmosphere decrease with increasing elevation angle. The tropospheric range error is frequency independent while ionospheric range error is inversely proportional to frequency squared. With no attempt at correction the tropospheric range bias is approximately 24 meters at 5° elevation. With a correction based only upon the worldwide standard atmosphere ($N_s$ = 313.0), this range error can be reduced to less than 0.5 meter at 5° elevation (Figure 10) for any of the typical tracking areas cited in Table 1. For a daytime ionosphere a maximum range error of 0.5 meter RMS can occur at 5° elevation at frequencies below 3.5 kMc for a 240 km earth orbit and below 10 kMc for vehicle heights at or above 500 km. For a nighttime

ionosphere a maximum range error of 0.5 meters RMS can occur at 5° elevation at frequencies below 2.0 kMc for a 240 km earth orbit and below 5.0 kMc for vehicle heights at or above 500 km (Figure 19). At lunar distances the range bias is determined by the uncertainty in the velocity of light of one part in $10^6$ which results in a bias on the order of 380 meters.

Short-term range fluctuations (period of fluctuation up to 10 minutes) decrease with increasing elevation angle and, for the troposphere, can be attributed primarily to the effects of cloud cover. Estimates of tropospheric range fluctuations at 5° elevation range from 0.5 meters RMS for heavy cumulus cover to 0.02 cm RMS for clear dry air. At 20° elevation the corresponding estimates are 0.25 meter RMS and 0.01 cm RMS (Table 2). Above 1 kMc the range fluctuation error due to the ionosphere at an elevation of 10° would not be expected to exceed 0.2 meter RMS even under worst case daytime conditions (Figure 21).

*Range Rate*

Range-rate bias due to the atmosphere decreases with increasing elevation angle. The troposphere introduces biasing for both earth orbit and lunar distance (or beyond) space travel. Above 1 kMc the ionosphere need only be considered for the case of earth orbit. In earth orbit there are two major sources of range-rate bias. The first has to do with the path change through the troposphere during the range-rate measurement interval and leads to a range-rate bias on the order of 50 cm per second at 5° elevation. If a correction is made based on the best yearly average of $N_s$ this can be reduced to 5 cm per second. A correction based on the best daily average reduces the error to essentially zero (Figure 11). The second range-rate bias source for an earth orbit through the ionosphere is due to the difference in angle between the refracted ray and the line-of-sight as measured at the vehicle. At 1 kMc the maximum error will be on the order of 100 cm per second at 0° elevation and 60 cm per second at 15° elevation. These values are reduced by a factor of approximately three for nighttime operation.

For space flight beyond the ionosphere, the error in local ray angle is not significant and the primary error source is the troposphere. At lunar distances the earth's rotation of $7 \times 10^{-5}$ radian per second introduces a tropospheric bias on the order of 2 cm per second at 5° elevation (Figures 13 and 14) independent of operating frequency.

## Influence of the Atmosphere at the Nominal Apollo Unified S-Band Frequency of 2 kMc

Tables 4 through 7 indicate the remaining error which can be expected after correction at a frequency of 2 kMc for day or night operation for both earth orbit and lunar distances.

Table 4

Expected Error in Measurement Due to Propagation Through the Earth's Atmosphere at 2 kMc.*

| Type of Correction | RMS Elevation Angle (mr) | | | RMS Range (meters) | | | RMS Range-Rate (cm/sec) | | |
|---|---|---|---|---|---|---|---|---|---|
| | Bias | Noise | | Bias | Noise | | Bias | Noise | |
| | | Clear Normal Air | Heavy Cumulus | | Clear Normal Air | Heavy Cumulus | | Average Cloud Cover | Heavy Cloud Cover |
| None | 4 | 0.02 | 0.4 | 25 | 0.01 | 0.5 | 75 | 0.022 | 0.075 |
| Yearly Average | 0.3 | 0.02 | 0.4 | 2.3 | 0.01 | 0.5 | 30 | 0.022 | 0.075 |
| Daily Average | 0.1 | 0.02 | 0.4 | 1.8 | 0.01 | 0.5 | 25 | 0.022 | 0.075 |

*Daytime ionosphere
Earth orbit h ≐ 200 km
5° elevation
$\dot{R}$ noise for 1 sec integration

Table 5

Expected Error in Measurement Due to Propagation Through the Earth's Atmosphere at 2 kMc.*

| Type of Correction | RMS Elevation Angle (mr) | | | RMS Range (meters) | | | RMS Range-Rate (cm/sec) | | |
|---|---|---|---|---|---|---|---|---|---|
| | Bias | Noise | | Bias | Noise | | Bias | Noise | |
| | | Clear Normal Air | Heavy Cumulus | | Clear Normal Air | Heavy Cumulus | | Average Cloud Cover | Heavy Cloud Cover |
| None | 4 | 0.02 | 0.4 | 24 | 0.004 | 0.5 | 58 | 0.022 | 0.075 |
| Yearly Average | 0.3 | 0.02 | 0.4 | 1.0 | 0.004 | 0.5 | 13 | 0.022 | 0.075 |
| Daily Average | 0.1 | 0.02 | 0.4 | 0.5 | 0.004 | 0.5 | 8 | 0.022 | 0.075 |

*Nighttime ionosphere
Earth orbit h ≐ 200 km
5° elevation
$\dot{R}$ noise for 1 sec integration

Table 6

Expected Error in Measurement Due to Propagation Through the Earth's Atmosphere at 2 kMc.*

| Type of Correction | RMS Elevation Angle (mr) | | | RMS Range (meters) | | | RMS Range-Rate (cm/sec) | | |
|---|---|---|---|---|---|---|---|---|---|
| | Bias | Noise | | Bias | Noise | | Bias | Noise | |
| | | Clear Normal Air | Heavy Cumulus | | Clear Normal Air | Heavy Cumulus | | Average Cloud Cover | Heavy Cloud Cover |
| None | 4 | 0.02 | 0.4 | 34 | 0.01 | 0.5 | 2 | 0.022 | 0.075 |
| Yearly Average | 0.3 | 0.02 | 0.4 | 10.5 | 0.01 | 0.5 | 0.2 | 0.022 | 0.075 |
| Daily Average | 0.1 | 0.02 | 0.4 | 10 | 0.01 | 0.5 | Bias <0.2 | 0.022 | 0.075 |

*Daytime ionosphere
Lunar orbit
5° elevation
$\dot{R}$ noise for 1 sec integration

Table 7

Expected Error in Measurement Due to Propagation Through the Earth's Atmosphere at 2 kMc.*

| Type of Correction | RMS Elevation Angle (mr) | | | RMS Range (meters) | | | RMS Range-Rate (cm/sec) | | |
|---|---|---|---|---|---|---|---|---|---|
| | Bias | Noise | | Bias | Noise | | Bias | Noise | |
| | | Clear Normal Air | Heavy Cumulus | | Clear Normal Air | Heavy Cumulus | | Average Cloud Cover | Heavy Cloud Cover |
| None | 4 | 0.02 | 0.4 | 27 | 0.004 | 0.5 | 2 | 0.022 | 0.075 |
| Yearly Average | 0.3 | 0.02 | 0.4 | 3.5 | 0.004 | 0.5 | 0.2 | 0.022 | 0.075 |
| Daily Average | 0.1 | 0.02 | 0.4 | 3 | 0.004 | 0.5 | Bias <0.2 | 0.022 | 0.075 |

*Nighttime ionosphere
Lunar orbit
5° elevation
$\dot{R}$ noise for 1 sec integration

## ACKNOWLEDGMENT

The author wishes to thank Dr. B. Kruger of the Mission Analysis Office, GSFC, for reviewing the manuscript and providing many helpful suggestions.

(Manuscript received December 23, 1965)

## REFERENCES

1. Barton, D. K., "Instrumentation Errors Due to Atmospheric Refraction," in: *New Data Reduction Methods to Improve Range Data (Papers Presented at the 4th Joint AFMTC-Range User Data Conference, Orlando Air Force Base, Florida, February 26-28, 1963)*, Patrick Henry Air Force Missile Base, Florida: Air Force Missile Test Center, 1964, pp. 285-322.

2. Anway, A. C., "Empirical Determination of Total Atmospheric Refraction at Centimeter Wavelengths by Radiometric Means," *NBS J. Res.*, Ser. D, 67D(2):153-160, March-April, 1963.

3. Bean, B. R., and Thayer, G. D., "Comparison of Observed Atmospheric Radio Refraction Effects with Values Predicted Through Use of Surface Weather Observations," *NBS J. Res.* Ser. D, 67D(3):273-285, May-June 1963.

4. Bean, B. R., and Thayer, G. D., "CRPL Exponential Reference Atmosphere," National Bureau of Standards Monograph No. 4, October 29, 1959.

5. Crane, R. K., "Ray Tracings in Cloud Cross-Sections for a Long Baseline Interferometer," in: *Proceedings of the Third Tropospheric Refraction Effects Meeting*, Vol. I, Bedford, Mass: Mitre Corp., November, 1964.

6. Martin, C. F., "Accuracy of Tropospheric Refraction Correction Procedures," in: *Proceedings of the Second Tropospheric Refraction Effects Technical Review Meeting,* Vol. II, Bedford, Mass.: Mitre Corp., April 1964, pp. 233-237.

7. Bean, B. R., Horn, J. D., and Ozanich, A. M., Jr., "Climatic Charts and Data of the Radio Refractive Index for the United States and the World," National Bureau of Standards Monograph No. 22, November 25, 1960.

8. Mason, J. F., "Modernizing the Missile Range; Part 2," *Electronics Magazine* 38(5):108-118, March 8, 1965.

9. Straiton, A. W., "Measurement of the Radio Refractive Index of the Atmosphere," in: *Advances in Radio Research,* Vol. 1, ed. by J. A. Saxton, London: Academic Press, 1964, pp. 2-50.

10. Clark, H. E., "Recommendations Concerning the Corrections of Radar Elevation Angles for Effects on Atmospheric Refraction," *Memorandum for Record, Data Operations Branch,* GSFC, 6 February 1963.

11. Atwood, J. G., "Phase I Report Determination of Optical Technology Experiments for a Satellite," *Engineering Report No. 7846,* Norwalk, Conn: Perkin-Elmer, Electro-Optical Division, November 1964, p. 14.

12. Barton, D. K., "Radar System Analysis," Englewood Cliffs, N. J.: Prentice Hall, 1964.

13. Millman, G. H., "Atmospheric and Extra Terrestrial Effects on Radio Wave Propagation," Syracuse, New York: G. E. Missile Detection Systems, Technical Information Services, 1960.

14. Donegan, J. J., "Apollo Mission Profile," in: *Proceedings of the Apollo Unified S-Band Technical Conference, Goddard Space Flight Center, July 14-15, 1965,* NASA Special Paper SP-87, 1965.

15. Sjogren, W. L., and Trask, D. W., "Radio Tracking of the Mariner and Range Missions and its Implications," JPL Technical Memorandum No. 312-517, Pasadena, Calif.; Jet Propulsion Laboratory, 15 March 1965, p. 32.

16. "Report of Ad Hoc Panel on Electromagnetic Propagation," in: *National Academy of Sciences Final Report,* ed. by D. K. Barton, Washington: National Academy of Sciences, February, 1963.

17. "Ionospheric Radio Propagation," National Bureau of Standards Circular 462, June 25, 1948.

18. Ramo, S., and Whinnery, J. R., "Fields and Waves in Modern Radio," New York: John Wiley, 1953, pp. 46-48.

19. "Doppler Propagation Study," WDL TR1993, Palo Alto, Calif.: Philco Corporation, Western Development Laboratories, January 1963.

20. Mendonca, F. D., "Ionospheric Electron Content and Variations Measured by Doppler Shifts in Satellite Transmissions," *J. Geophys. Res.* 67(6):2315-2337, June 1962.

21. Meecham, W. C., "Satellite Signal Fluctuations Caused by Ionospheric Irregularity," *J. Geophys. Res.* 69(15):3175-3185, August 1, 1964.

22. Pfister, W., and Keneshea, T. J., "Ionospheric Effects on Positioning of Vehicles at High Altitudes," AFCRC-TN-56-203, Bedford, Mass.: Air Force Cambridge Research Center, Ionospheric Physics Laboratory, March 1956.

Appendix A

## Glossary

For purposes of this paper the following definitions are employed:

REFRACTIVITY

The refractivity of the atmosphere is represented by N, where

$$N = (n - 1)\, 10^6 ,$$

$n$ = index of refraction.

TROPOSPHERE

That region of the earth's atmosphere immediately adjacent to the earth and extending upwards about 30 km.

FREESPACE REGION

The index of refraction of the earth's atmosphere between 30 km and 85 km is for all practical purposes unity and hence this region can be considered as "free space."

IONOSPHERE

That region of the earth's atmosphere in which the constituent gases are ionized by radiation from outer space. This region extends from about 85 km to 1000 km above the earth.

ATMOSPHERE

The gaseous matter surrounding the earth, including both the troposphere and ionosphere.

*"The aeronautical and space activities of the United States shall be conducted so as to contribute . . . to the expansion of human knowledge of phenomena in the atmosphere and space. The Administration shall provide for the widest practicable and appropriate dissemination of information concerning its activities and the results thereof."*

—NATIONAL AERONAUTICS AND SPACE ACT OF 1958

# NASA SCIENTIFIC AND TECHNICAL PUBLICATIONS

TECHNICAL REPORTS: Scientific and technical information considered important, complete, and a lasting contribution to existing knowledge.

TECHNICAL NOTES: Information less broad in scope but nevertheless of importance as a contribution to existing knowledge.

TECHNICAL MEMORANDUMS: Information receiving limited distribution because of preliminary data, security classification, or other reasons.

CONTRACTOR REPORTS: Technical information generated in connection with a NASA contract or grant and released under NASA auspices.

TECHNICAL TRANSLATIONS: Information published in a foreign language considered to merit NASA distribution in English.

TECHNICAL REPRINTS: Information derived from NASA activities and initially published in the form of journal articles.

SPECIAL PUBLICATIONS: Information derived from or of value to NASA activities but not necessarily reporting the results of individual NASA-programmed scientific efforts. Publications include conference proceedings, monographs, data compilations, handbooks, sourcebooks, and special bibliographies.

***Details on the availability of these publications may be obtained from:***

SCIENTIFIC AND TECHNICAL INFORMATION DIVISION

NATIONAL AERONAUTICS AND SPACE ADMINISTRATION

**Washington, D.C. 20546**